Autoreactive antibodies control blood glucose by regulating insulin homeostasis

Timm Amendt[a], Gabriele Allies[a], Antonella Nicolò[a], Omar El Ayoubi[a], Marc Young[a], Tamás Röszer[b], Corinna S. Setz[a], Klaus Warnatz[c], and Hassan Jumaa[a,1]

[a]Institute of Immunology, Ulm University Medical Center, 89081 Ulm, Germany; [b]Institute of Neurobiology, Ulm University, 89081 Ulm, Germany; and [c]Center for Chronic Immunodeficiency, University Hospital Freiburg, Albert-Ludwigs-Universität Freiburg, 79104 Freiburg, Germany

Edited by Michael Reth, Institute of Biology III, Faculty of Biology, Albert-Ludwigs-Universitat Freiburg, Freiburg, Germany; received August 25, 2021; accepted December 23, 2021

Homeostasis of metabolism by hormone production is crucial for maintaining physiological integrity, as disbalance can cause severe metabolic disorders such as diabetes mellitus. Here, we show that antibody-deficient mice and immunodeficiency patients have subphysiological blood glucose concentrations. Restoring blood glucose physiology required total IgG injections and insulin-specific IgG antibodies detected in total IgG preparations and in the serum of healthy individuals. In addition to the insulin-neutralizing anti-insulin IgG, we identified two fractions of anti-insulin IgM in the serum of healthy individuals. These autoreactive IgM fractions differ in their affinity to insulin. Interestingly, the low-affinity IgM fraction (anti-insulin IgM^{low}) neutralizes insulin and leads to increased blood glucose, whereas the high-affinity IgM fraction (anti-insulin IgM^{high}) protects insulin from neutralization by anti-insulin IgG, thereby preventing blood glucose dysregulation. To demonstrate that anti-insulin IgM^{high} acts as a protector of insulin and counteracts insulin neutralization by anti-insulin IgG, we expressed the variable regions of a high-affinity anti-insulin antibody as IgG and IgM. Remarkably, the recombinant anti-insulin IgM^{high} normalized insulin function and prevented IgG-mediated insulin neutralization. These results suggest that autoreactive antibodies recognizing insulin are key regulators of blood glucose and metabolism, as they control the concentration of insulin in the blood. Moreover, our data suggest that preventing autoimmune damage and maintaining physiological homeostasis requires adaptive tolerance mechanisms generating high-affinity autoreactive IgM antibodies during memory responses.

B cells | autoimmunity | IgM | IgG | aging

Maintaining homeostasis is a complex interplay of the hormone system, immune system, and metabolism (1, 2). B cells and antibody-secreting plasma cells are fundamentally involved in immunity, as they are able to recognize an enormous number of epitopes due to random rearrangement of variable (V), diversity (D), and joining (J) gene segments (3, 4). B cells originate from hematopoietic stem cells in the bone marrow, where, in early stages, two IgM-heavy chains and two surrogate light chains form the pre–B cell receptor (pre-BCR) (5). Autoreactive specificities are believed to be subjected to removal by clonal deletion or receptor editing (6–8). Immature B cells expressing an IgM-class B cell antigen receptor (IgM–BCR) leave the bone marrow and home to the spleen, where they mature further (9). The maturation of B cells in the periphery includes downmodulation of IgM and up-regulation of the IgD-class BCR (10–13). Recently, our group has shown that the IgD-class BCR is exclusively responsive to polyvalent antigen (10) and that the modulation of IgG responses via soluble (auto)-antigens in vivo also occurs in an IgD-dependent manner (14). Furthermore, mice as well as humans harbor a large number of autoreactive IgD^{+} B cells (15, 16) of which the function remains unclear.

Autoreactive B cells and plasma cells that secrete autoantibodies of the IgG isotype might cause autoimmune diseases such as systemic lupus erythematosus (17), type 1 diabetes (T1D) (18), or rheumatoid arthritis (19–21). Here, autoreactive IgG is capable of neutralizing its autoantigen or opsonizing it for further degradation or destruction by the innate immune system (22). Furthermore, autoantibody-containing immune complexes are able to induce inflammation (23, 24). Another class of autoreactive antibodies is represented by polyreactive natural IgM (nIgM) that has been extensively studied (25, 26). nIgM is secreted by B1-B cells and known to clear oxidized lipids and other potentially harmful self-molecules (27). Thus, nIgM is able to suppress sterile inflammation and therefore required to be secreted in an antigen-encounter–independent fashion (25, 26). In sum, autoreactive IgG and IgM are known to remove self-targets, and disease outbreak is dependent on the isotype present.

In mice, we recently identified an autoreactive IgM class that is able to bind and stabilize its cognate antigen. We refer to this class of autoreactive IgM as protective regulatory IgM (PR-IgM) (28). A key characteristic of PR-IgM is high affinity and monospecificity to its antigen. PR-IgM is induced in the course of autoreactive immune responses and results in the protection of cognate autoantigen from degradation or uptake by macrophages. We refer to this phenomenon as adaptive tolerance. However, the presence of PR-IgM in humans is yet unclear.

Significance

The random nature of antibody repertoire generation includes the potential of producing autoantibodies recognizing self-structures. It is believed that establishing immunological tolerance and prevention of autoimmune diseases require the removal of antibody specificities recognizing self. Using insulin as a common and physiologically important autoantigen, we show that anti-insulin antibodies associated with autoimmune diabetes can readily be detected in mice and humans and are involved in the physiological regulation of blood glucose levels. Importantly, human high-affinity, anti-insulin IgM antibodies protect insulin from autoimmune degradation by anti-insulin IgG antibodies. Thus, in contrast to the proposed negative selection, self-recognition and the production of highly autoreactive IgM antibodies are important for tolerance induction.

Author contributions: H.J. designed research; T.A., G.A., A.N., O.E.A., M.Y., T.R., C.S.S., and K.W. performed research; K.W. contributed new reagents/analytic tools; T.A. analyzed data; and T.A. and H.J. wrote the paper.

Competing interest statement: T.A., M.Y., and H.J. have filed patent applications for the use of protective-regulatory insulin antibodies.

This article is a PNAS Direct Submission.

[1]To whom correspondence may be addressed. Email: hassan.jumaa@uni-ulm.de.

This article contains supporting information online at http://www.pnas.org/lookup/suppl/doi:10.1073/pnas.2115695119/-/DCSupplemental.

Published February 7, 2022.

Here, we show that PR-IgM specific for insulin accumulates with age in humans and is able to stabilize insulin in vivo. Furthermore, we show that autoreactive IgG in humans and mice is involved in the fine-tuning of metabolic homeostasis by regulating physiological insulin concentrations. In fact, antibody deficiency is associated with dysglycemia, which is restored after the transfer of total IgG from healthy donors.

Results

Anti-insulin IgG Regulates Blood Glucose Concentration. Using insulin as a common and important autoantigen, we recently developed a simple animal model for testing the induction of autoreactive antibody responses (28). The heterodimeric hormone insulin consists of an alpha and beta chain that are covalently linked via disulfide bonds. In addition, the alpha chain also contains an internal disulfide bond (29). Importantly, we were able to show that the presence of polyvalent insulin was sufficient to induce an autoimmune response which can easily be monitored by deregulated glucose concentration in blood and urine similar to diabetes (30, 31). During these experiments, we noticed that a considerable amount of total IgG isolated from naıve wildtype (WT) mice was reactive to insulin (Fig. 1 *A* and *B*). To confirm these data, we performed ELISpot assays and found that anti-insulin IgG-secreting plasma cells are present in the spleen of WT mice (Fig. 1*C*). When we measured the blood glucose concentrations in WT and B cell–deficient mice [mb1-deficient mice (32)], which cannot produce antibodies (*SI Appendix*, Fig. S1), we detected a surprising difference. Unexpectedly, the mb1-deficient mice showed abnormally reduced blood glucose levels as compared to WT controls (Fig. 1*D*). In full agreement, enzyme-linked immunosorbent assay (ELISA) experiments revealed significantly increased serum insulin concentrations in mb1-deficient mice compared to WT mice (*SI Appendix*, Fig. S2). Notably, the mb1-deficient mice show comparable body weight to that of WT mice as determined in previous investigations.

To test whether this abnormal decrease is caused by antibody deficiency, we injected total IgG from WT mice, or an anti-insulin IgG-depleted control of the same total IgG, intravenously (i.v.) into mb1-deficient mice. We found that blood glucose concentration increased with the total murine IgG but not with the anti-insulin IgG-depleted control (Fig. 1*E*). In order to test the consequence of reduced steady-state blood glucose on the fitness, we performed wire hanging tests to assess motor function and found that mb1-deficient mice show significantly reduced wire hanging times as compared to WT controls. Importantly, this deficit in wire hanging times was restored after the intravenous injection of total murine IgG (Fig. 1*F*). In addition, mb1-deficient mice also showed dysregulated blood glucose levels after rotarod exercise (*SI Appendix*, Fig. S3).

Since total IgG preparations from healthy donors are often used as intravenous immunoglobulin (IVIg) infusions in the treatment of immunodeficiency (33), we tested the presence of anti-insulin IgG in these preparations. All preparations contained substantial amounts of anti-insulin IgG. However, the anti-insulin IgG concentration seemed to be increased if the United States was the country of origin (*SI Appendix*, Fig. S4). Since insulin is highly conserved between man and mouse, we injected human IVIg into the mb1-deficient mice and detected a decrease in insulin concentration (Fig. 1*G*). Notably, the IVIg preparations used for in vivo studies did not contain sugars as stabilizers and thus cannot affect blood glucose levels directly (33). Moreover, injecting 50 μg human IVIg into WT mice led to increased blood glucose, and this effect required anti-insulin IgG since the depletion of the anti-insulin IgG from human IVIg prevented the IVIg-induced increase in blood glucose (Fig. 1*H* and *SI Appendix*, Fig. S5).

To test whether the IVIg injection shows similar results in human CVID (common variable immunodeficiency) patients suffering from antibody deficiency (*SI Appendix*, Table S1), we monitored blood glucose before and after IVIg injection. Similar to mb1-deficient mice, antibody-deficient patients showed reduced blood glucose concentrations as compared to healthy donors. Importantly, the concentration of serum glucose increased and reached normal levels briefly after the following IVIg infusion (Fig. 1*I*). Furthermore, immunodeficiency patients that received IVIg showed decreased serum insulin levels immediately after the infusion (*SI Appendix*, Fig. S6).

To show that the anti-insulin IgG present in IVIg is specific for insulin, we determined the affinity via biolayer interferometry (BLI). A dissociation constant of 10^{-11} suggests that the anti-insulin IgG is highly specific for insulin (Fig. 1*J*).

These data suggest that anti-insulin IgG is present in healthy individuals and might be required for the regulation of blood glucose concentration.

Blood Glucose Is Regulated by Antibody Class and Affinity. To further confirm our finding regarding the presence of anti-insulin antibodies in healthy individuals, we monitored the level of anti-insulin IgG and IgM in the blood of different age groups. We found that anti-insulin IgG was similar in young and aged humans (Fig. 2*A*), while anti-insulin IgM seemed to decline with age in males and females (Fig. 2*B*). Interestingly, the human anti-insulin IgM recognizes multiple epitopes of insulin (*SI Appendix*, Fig. S7).

In agreement with the high specificity, the anti-insulin IgG showed no binding to any cellular structure in indirect immunofluorescence assay (IIFA) on HEp-2 cells, which is a commonly used method for the detection of antinuclear antibodies (ANA) (34) (*SI Appendix*, Fig. S8). The anti-insulin IgM, however, consisted of two fractions that can be biochemically separated according to their affinity to insulin (35). Low-affinity anti-insulin IgM (IgM^{low}) is eluted from the insulin column at a higher pH (5) as compared to high-affinity anti-insulin IgM (IgM^{high}), which requires acidic conditions (pH = 2.8) for elution (Fig. 2*C*). The IgM^{low} fraction shows polyreactivity as detected by binding to nuclear structures in IIFA and double-stranded DNA (dsDNA) binding in ELISA, whereas the IgM^{high} fraction is virtually negative in these assays (Fig. 2 *D* and *E*). Furthermore, we confirmed the difference in affinity by performing BLI assays and found that IgM^{low} and IgM^{high} possess a dissociation constant of 10^{-7} and 10^{-10}, respectively (Fig. 2*F*). To test the effect of the different IgM fractions on glucose metabolism, we injected identical amounts of insulin-reactive IgM^{low} and IgM^{high} into WT mice. Increased blood glucose was observed within 2 h after injection in the mice that received IgM^{low}, whereas IgM^{high} did not significantly alter blood glucose levels (Fig. 2*G*). Moreover, we tested whether IgM^{high} plays a regulatory role under conditions of abnormally increased insulin concentrations that may cause hypoglycemia. To this end, we injected 0.5 μg insulin in combination with IgM^{high} or unspecific IgM isotype control. Strikingly, the presence of anti-insulin IgM^{high}, but not the IgM isotype control, prevented the drastic decrease in blood glucose that occurred immediately after insulin injection (Fig. 2*H*). To further test the regulatory role of IgM^{high} in protecting insulin from IgG-mediated degradation, we combined the anti-insulin IgM^{high} with anti-insulin IgG purified from IVIg preparations. The data show that the anti-insulin IgM^{high} acts as PR-IgM preventing the IgG-mediated neutralization of insulin, which results in increased blood glucose levels (Fig. 2*I* and *SI Appendix*, Fig. S9). These data suggest that anti-insulin IgM^{high} is important for regulating glucose metabolism by protecting insulin from IgG-mediated neutralization and by binding excessive insulin, thereby preventing drastic declines in insulin concentrations. The decrease in insulin-reactive IgM with age

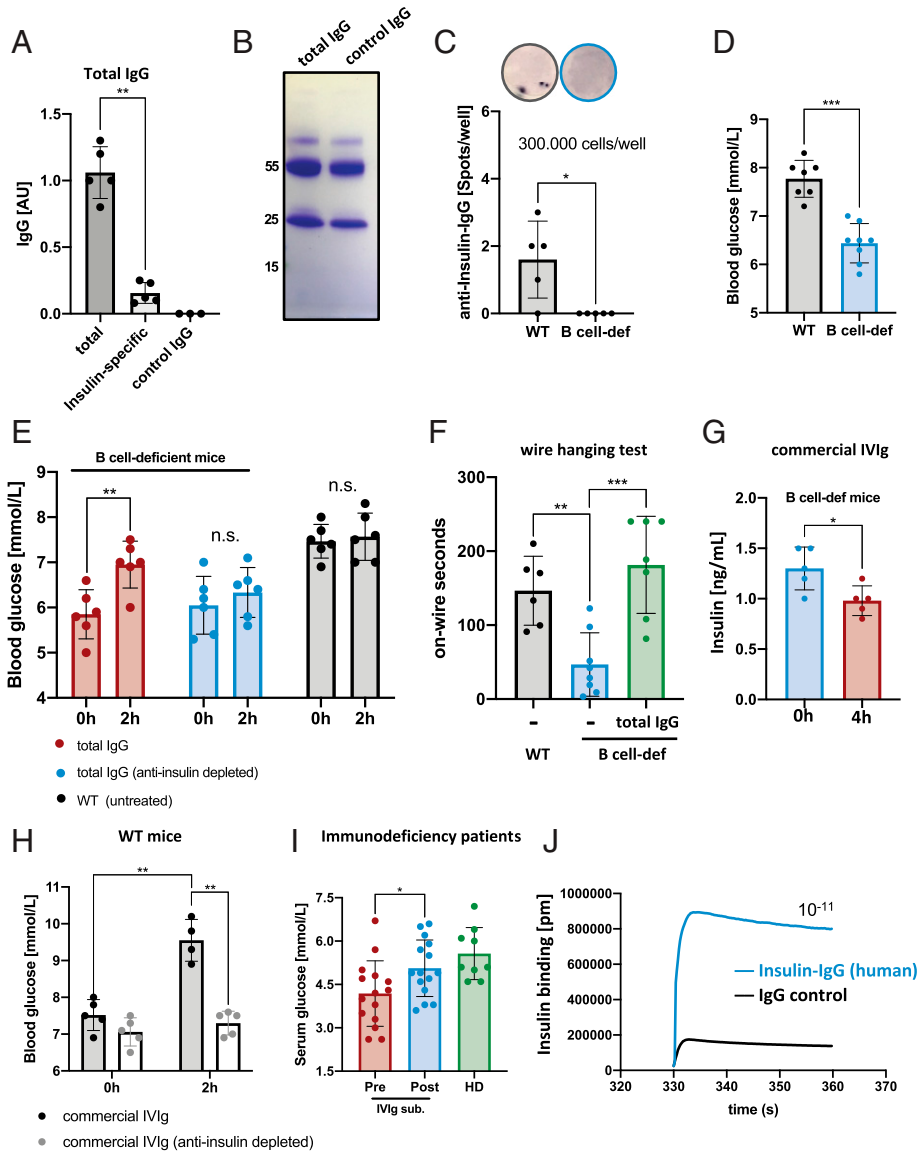

Fig. 1. Autoantibodies are required to balance homeostasis in mice. (*A*) Insulin-specific IgG concentrations of different IgG pulldowns measured by ELISA (coating: native insulin). Total: total IgG pulldown via protein G ($n = 5$), Insulin-specific: IgG pulldown via insulin bait column ($n = 5$), control IgG ($n = 3$). Mean ± SD, statistical significance was calculated using Kruskal–Wallis test. Arbitrary unit (AU) = μg/mL, $^{**}P < 0.01$. (*B*) Coomassie-stained SDS-PAGE showing total IgG (pulldown from serum) and IgG control (total IgG depleted for anti-insulin IgG) under reducing conditions (β-mercaptoethanol). The image is representative of three independent experiments. The marker on the left is shown in kilodaltons (kDa). (*C*) Anti-insulin IgG–secreting splenocytes of naïve WT and mb1-deficient mice measured by ELISpot (coating: native insulin). The cells were seeded at 300,000 cells/well and incubated for 48 h ($n = 5$/group), mean ± SD, statistical significance was calculated using Mann–Whitney *U* test. Top images of wells are representative of three independent experiments. $^{*}P < 0.05$. (*D*) Blood glucose levels of naïve WT and mb1-deficient mice measured with a commercial blood glucose monitor (mmol/L). Mean ± SD, statistical significance was calculated using Mann–Whitney *U* test. $^{***}P < 0.001$. (*E*) Blood glucose levels of WT and mb1-deficient mice (red: $n = 6$, blue: $n = 6$) i.v. injected with 200 μg total IgG, IgG depleted for anti-insulin IgG measured at indicated hours. Mean ± SD, statistical significance was calculated using repeated measure ANOVA test. $^{**}P < 0.01$, n.s. = not significant. (*F*) Motor function of WT and mb1-deficient mice as measured by wire-hanging test (on-wire seconds). Gray: WT untreated ($n = 6$), blue: mb1-deficient untreated ($n = 8$), green: mb1-deficient injected with 200 μg total IgG ($n = 7$). Mean ± SD, statistical significance was calculated using Kruskal–Wallis test. $^{**}P < 0.01$, $^{***}P < 0.001$. (*G*) Serum insulin concentrations of mb1-deficient mice injected with 200 μg commercial human IVIg as measured by ELISA at indicated time points ($n = 5$). Mean ± SD, statistical significance was calculated using Mann–Whitney *U* test. $^{*}P < 0.05$. (*H*) Blood glucose levels of WT mice injected with 200 μg commercial human IVIg (black: $n = 5$ for 0 h, $n = 4$ for 2 h post-injection) and commercial human IVIg depleted for anti-insulin IgG (gray: $n = 5$) measured by a commercial blood glucose monitor (mmol/L) at indicated hours. Mean ± SD, statistical significance was calculated using repeated measure ANOVA test. $^{**}P < 0.01$. (*I*) Serum glucose levels of immunodeficiency patients (CVID) that received commercial IVIg before (pre, $n = 15$) and after (post, $n = 15$) infusion compared to healthy donors (HD, $n = 9$). Mean ± SD, statistical significance was calculated using Kruskal-Wallis test. $^{*}P < 0.05$. (*J*) Insulin-binding affinity of human anti-insulin IgG determined by BLI. The K_d (dissociation constant) was calculated by using the K_a (association constant): $1/K_a$. Data are representative of three independent experiments performed in three dilution steps per sample.

(Fig. 1*A*) prompted us to test whether the anti-insulin IgM^{high} or IgM^{low} is affected by this decrease. We determined the amount of anti-insulin IgM^{high} or IgM^{low} in young and old healthy donors and found that the ratio of anti-insulin IgM^{high} increases with age (Fig. 2*J*).

Together, these data suggest that glucose metabolism is regulated by different classes of antibodies and that anti-insulin IgM^{high} acts as PR-IgM that regulates glucose metabolism by regulating insulin homeostasis, which seems to be particularly important with age.

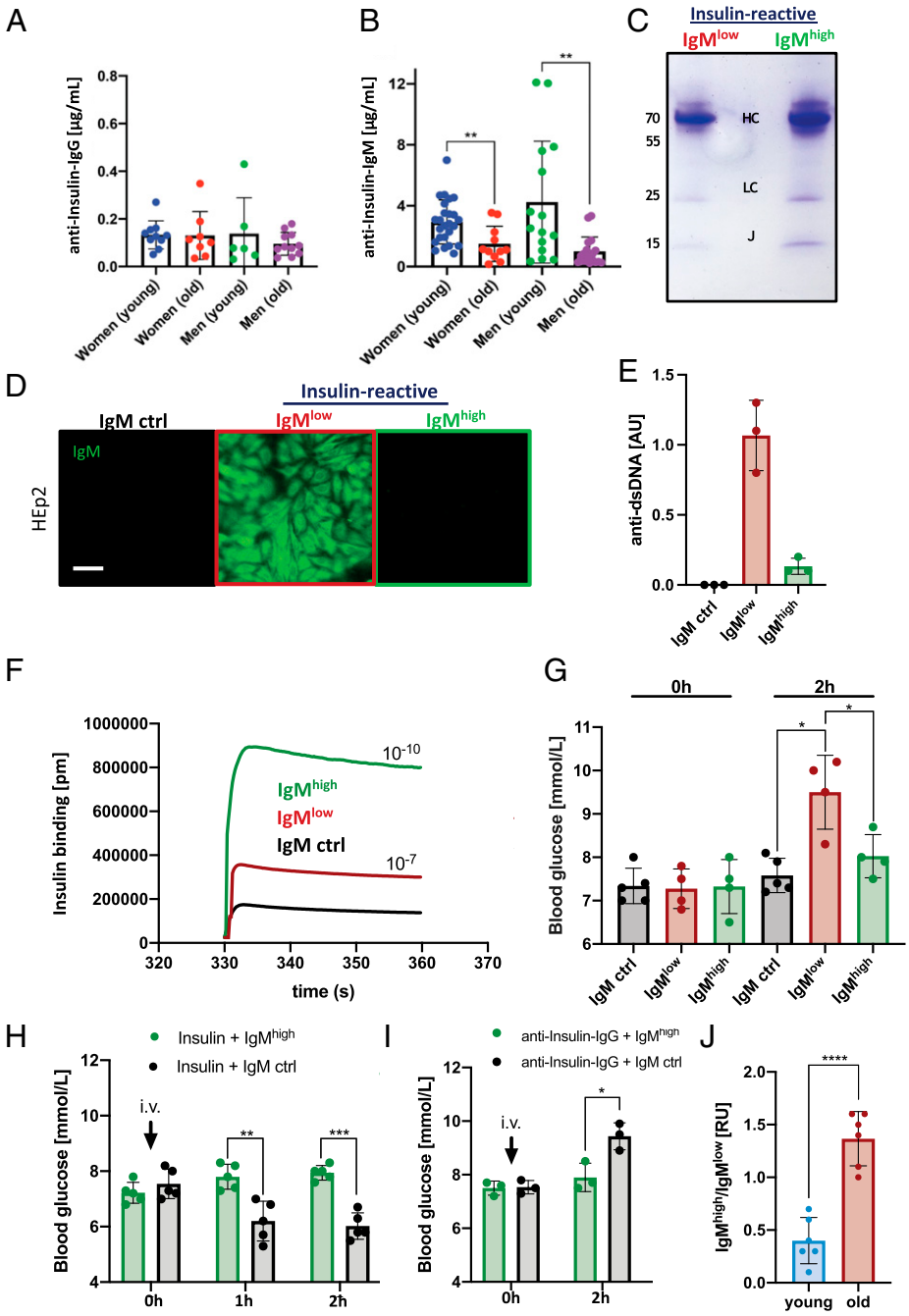

Fig. 2. Neutralizing and PR-IgM is present in humans. (*A* and *B*) Serum anti-insulin IgG (*A*) and IgM (*B*) concentrations of young (<30 y) and old (>65 y) human individuals measured by ELISA (coating: native Insulin). Women (young): $n = 25$, women (old): $n = 11$, men (young): $n = 15$, men (old): $n = 12$. Mean ± SD, statistical significance was calculated using Kruskal–Wallis test. $^{**}P < 0.01$. (*C*) Coomassie-stained SDS-PAGE showing low-affinity anti-insulin IgM (red) and high-affinity anti-insulin IgM (green) after purification under reducing conditions (β-mercaptoethanol). Image is representative of three independent experiments. Marker on the left is shown in kDa, HC (heavy chain): 70 kDa, LC (light chain): 25 kDa, J (J-chain): 15 kDa. (*D*) HEp2 slides showing nuclear structure–reactive IgM (ANA) of insulin-reactive IgM pulldowns. Black: monoclonal IgM control ($n = 6$), red: low-affinity anti-insulin IgM ($n = 6$), green: high-affinity anti-insulin IgM ($n = 6$). (Scale bar: 10 µm.) Green fluorescence indicates HEp2 cell binding. Images are representative of four independent experiments. (*E*) Anti-dsDNA IgM concentrations of insulin-specific IgM pulldowns as measured by ELISA (coating: calf-thymus dsDNA). IgM control (ctrl, $n = 3$), IgM^{low} ($n = 3$), IgM^{high} ($n = 3$). Mean ± SD, statistical significance was calculated using Kruskal–Wallis test (all comparisons were n.s.). (*F*) Insulin-binding affinity of human anti-insulin IgM pulldowns determined by BLI. The K_d (dissociation constant) was calculated by using the K_a (association constant): $1/K_a$. Data are representative for three independent experiments performed in three dilution steps. (*G*) Blood glucose levels of WT mice i.v. injected with 100 µg human insulin-specific IgM and human IgM control (black: $n = 5$, red: $n = 4$, green: $n = 4$). Mean ± SD, statistical significance was calculated using repeated measure ANOVA test. $^{*}P < 0.05$. (*H* and *I*) Blood glucose levels of WT mice intravenously injected with 100 µg human insulin-specific IgM (uppercase refers to affinity fraction) and human IgM control together with 500 ng native insulin (insulin + IgM^{high}, green: $n = 5$; insulin + IgM control: $n = 5$) (*H*) or together with 100 µg human anti-insulin IgG ($n = 3$/group) (*I*). Mean ± SD, statistical significance was calculated using repeated measure ANOVA test. $^{*}P < 0.05$, $^{**}P < 0.01$, $^{***}P < 0.001$. (*J*) Ratio of insulin-specific IgM of young (<30 y, $n = 6$) and old (>65 y, $n = 6$) individuals as determined by ELISA. Insulin-specific IgM was isolated via insulin bait columns prior to ELISA experiments. Mean ± SD, statistical significance was calculated using Kruskal–Wallis test. $^{****}P < 0.0001$.

Induction of Anti-insulin Antibodies by Insulin Complexes. The presence of anti-insulin antibodies raises the question about the potential mechanisms of an adaptive generation of autoreactive antibodies. We have recently shown that autoreactive antibodies can easily be elicited by polyvalent antigen in classical immunization experiments involving adjuvants (28). To show that complexed autoantigen is capable of inducing autoreactive antibody responses independent of any adjuvants, we incubated insulin with a typical homobifunctional crosslinker, 1,2-phenylene-bis-maleimide (36), which covalently binds to free sulfhydryl (SH) groups of cysteine in proteins, thereby cross-linking the protein of interest (Fig. 3*A*). Importantly, SH group–containing drugs were reported to induce anti-insulin autoantibodies (37–39). Moreover, increased pancreas activity and elevated insulin production result in the abnormal formation of disulfide bonds between insulin peptides, which may generate abnormal insulin forms that are more susceptible for SH group–mediated cross-linking, and thus complex formation, under conditions of oxidative stress (40–43). The homobifunctional cross-linking of insulin with 1,2-phenylene-bis-maleimide was tested in sodium dodecyl sulfate–polyacrylamide gel electrophoresis (SDS-PAGE), and the cross-linked insulin was purified using size-exclusion spin columns excluding monomeric and dimeric insulin (Fig. 3*B*). The insulin complexes were dialyzed and injected into WT mice (20 μg per mouse) without any additional adjuvants. As control, we performed a typical immunization using CpG as the adjuvant and streptavidin as a foreign carrier. We found that the insulin complexes lead to increased blood glucose levels and anti-insulin IgM at day 7 (d7) of treatment similar to the immunization (Fig. 3 *C* and *D*). Notably, the insulin complex itself did not affect blood glucose levels shortly after injection, suggesting that the biological activity of insulin is abrogated by protein complex formation (*SI Appendix*, Fig. S10). In addition, insulin-reactive IgG was detectable by ELISA on d14 and d26 (*SI Appendix*, Fig. S11). The repeated injection of insulin complexes at d21 resulted in further deregulation of glucose metabolism (Fig. 3*E*). Thus, we injected anti-insulin IgM^{high} at d22, 1 d after the injection of the insulin complexes. We found that anti-insulin IgM^{high} was able to prevent the blood glucose deregulation induced by the injection of insulin complexes (Fig. 3*E*).

Our previous work suggests that anti-insulin IgG induces pancreas inflammation and infiltration by macrophages and granulocytes (28). Next, we tested whether anti-insulin IgM^{high} was also able to prevent IgG-mediated pancreas inflammation. We found that anti-insulin IgM^{high} prevents pancreas inflammation and damage as shown by the decrease of macrophage ($CD11b^+/Ly6G^+$) and neutrophil ($Ly6G^+$) infiltration in the pancreas and the decrease of serum pancreatic lipase (Fig. 3 *F* and *G* and *SI Appendix*, Fig. S12).

As a mechanism for the protective role of anti-insulin IgM^{high} as compared to anti-insulin IgM^{low}, we proposed that the polyreactivity of the latter, which also binds dsDNA, induces the formation of immune complexes that can be phagocytosed by macrophages. In contrast, anti-insulin IgM^{high} is highly specific for insulin and does not form large immune complexes. We hypothesized that the inability of IgM^{high} to form large immune complexes results in poor phagocytosis by macrophages and therefore leads to a prolonged half-life of bound antigen. To test this, we incubated anti-insulin IgM^{high} or anti-insulin IgM^{low} with insulin in the presence of genomic dsDNA. Macrophages can phagocytose IgM immune complexes (44–46), and it is proposed that IgM-mediated phagocytosis is mediated by CD11b/CD18 but is independent of the FcμR, which binds to IgM but is mainly expressed by lymphocytes and not by macrophages (47–49). We found an increased binding/phagocytosis of anti-insulin IgM^{low} as compared to anti-insulin IgM^{high} (Fig. 3*H* and *SI Appendix*, Fig. S13). In addition, IgM^{high} was able to protect insulin from degradation, as the decline of insulin was greater in the supernatants containing anti-insulin IgM^{low} as compared to anti-insulin IgM^{high} antibodies (*SI Appendix*, Fig. S14).

These data show that anti-insulin antibodies can be generated under conditions activating the formation of insulin complexes, which results in deregulated glucose metabolism that can be counteracted by anti-insulin IgM^{high} that acts as PR-IgM.

Recombinant Anti-insulin IgM Regulates Blood Glucose. The results in Fig. 2 suggest that insulin-specific PR-IgM might be of great therapeutic interest, as it regulates insulin homeostasis and might prevent pancreas malfunction, both of which are essential for normal physiology and the prevention of diabetes. According to our data, an anti-insulin IgM can act as PR-IgM if it possesses high binding affinity to insulin and is not reactive to other autoantigens such as dsDNA or nuclear structures in IIFA. We hypothesized that a human insulin-specific IgG antibody can be converted into insulin-specific PR-IgM by exchanging the constant region.

Thus, we cloned and expressed a published human insulin-specific monoclonal antibody (50) as IgG1 (IgG_{MY}) and IgM (IgM_{MY}). To test the quality of our in vitro–produced antibodies, we assessed their glycosylation by PNGaseF treatment, which resulted in reduced molecular weight as compared to untreated controls suggesting a functional glycosylation (*SI Appendix*, Fig. S15). We determined the affinity of both IgG and IgM to be 10^{-9} (K_D) (Fig. 4*A*). Almost no dsDNA binding was observed in ELISA, and no nuclear staining was observed in IIFA as compared to total human serum IgM (Fig. 4 *B* and *C*). Moreover, by injection into mice, we tested if the monomeric anti-insulin IgM is capable of protecting insulin from degradation. Anti-insulin IgG led to a blood glucose increase, which was abolished when monomeric IgM_{MY} was present (Fig. 4*D*).

To test whether the resulting recombinant human anti-insulin IgM_{MY} possesses protective regulatory functions, we coinjected it with insulin and found that anti-insulin IgM_{MY} prevents a drastic drop in glucose concentration induced by an excess of insulin (Fig. 4*E*). Moreover, anti-insulin IgM_{MY} protects insulin from anti-insulin IgG_{MY}–mediated neutralization, as it prevents the increase in blood glucose induced by anti-insulin IgG_{MY} (Fig. 4*F*). In addition, anti-insulin IgM_{MY} counteracts the leak of glucose into urine (Fig. 4*G*).

These data suggest that expressing a high-affinity insulin-specific antibody as IgM regulates insulin homeostasis, prevents a deregulation of blood glucose concentration, and might grant novel strategies for diabetes treatment.

Discussion

This study shows that autoreactive anti-insulin IgM and IgG antibodies are normally present in WT animals and in human subjects. Moreover, the presence of such autoantibodies is neither an accident nor a failure in negative selection, it is rather an important element in the regulation of insulin concentration and glucose metabolism. An even more surprising result is the finding that the affinity of autoreactive anti-insulin IgM determines the outcome of its interaction with insulin. A high-affinity anti-insulin IgM is protective, while low-affinity IgM is destructive. Since low-affinity IgM is positive in IIFA (HEp2) and recognizes additional autoantigens such as dsDNA, it is multispecific, while high-affinity IgM is monospecific, as it recognizes only insulin. The multispecific nature of the low-affinity IgM leads to the formation of larger immune complexes (28), which seems to accelerate insulin phagocytosis and, most likely, its degradation by macrophages, thereby leading to an increase in blood glucose levels. Obviously, the most unexpected finding is the protective role of the high-affinity IgM toward insulin, as

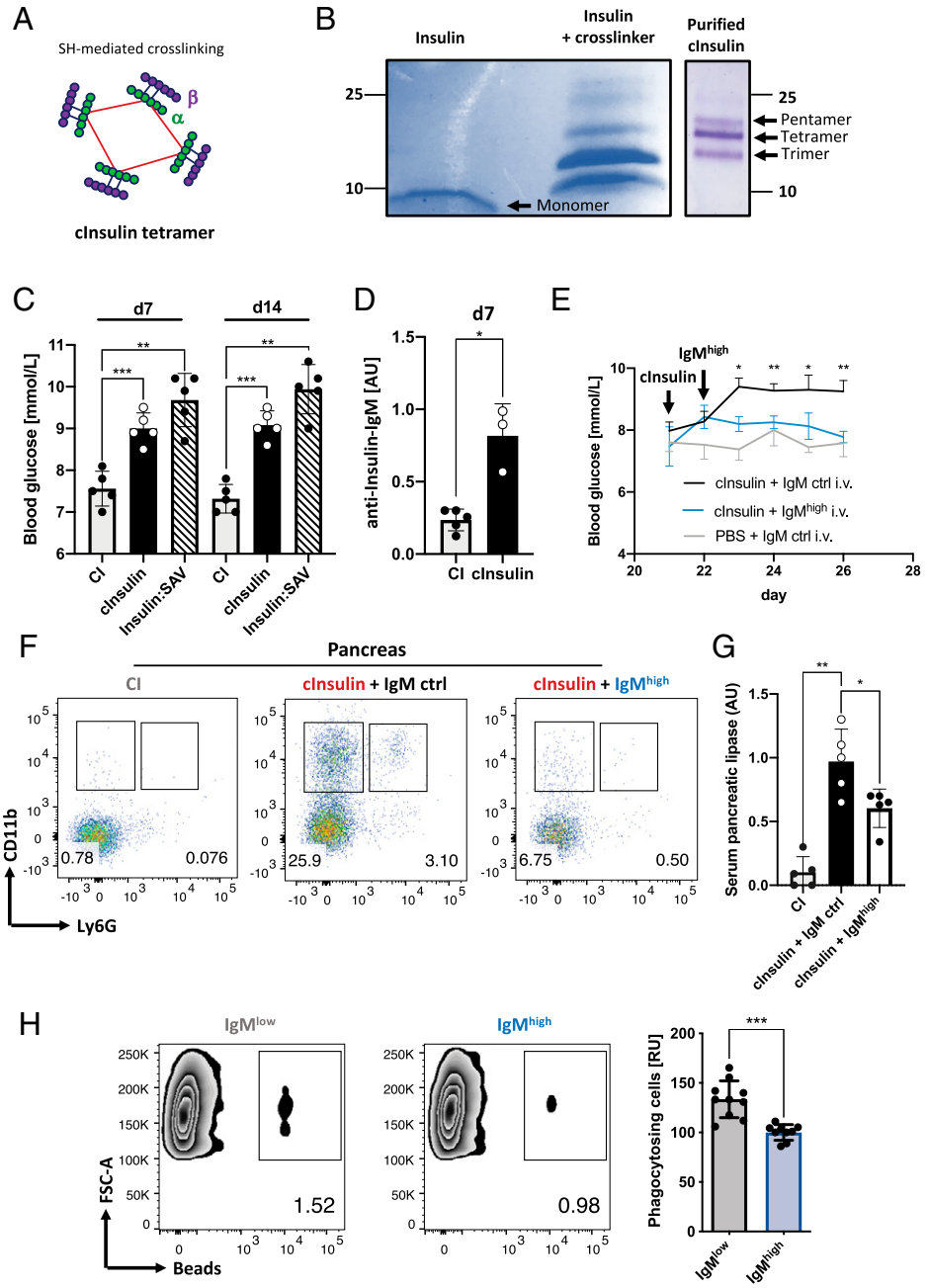

Fig. 3. Endogenous insulin complexes induce robust autoimmunity in mice. (*A*) Schematic illustration of insulin tetramers (cInsulin) generated by reactive SH group–mediated carbon–sulfur bond cross-linking via 1,2-phenylene-bis-maleimide. Black lines: endogenous disulfide bonds, red lines: cross-linking induced carbon–sulfur bonds. Alpha and beta chain of insulin are indicated by green and purple, respectively. (*B*) Coomassie-stained nonreducing BN-PAGE showing soluble insulin (6 kDa) and cross-linked insulin (>6 kDa). cInsulin complexes after purification with a 10-kDa size exclusion column are on *Right*. Images are representative of three independent experiments. Markers on the left/right site indicate band size in kDa. (*C*) Blood glucose levels of WT mice i.p. injected with PBS (CI: $n = 5$), cInsulin ($n = 5$), or Insulin:SAV (bio-Insulin:streptavidin, $n = 5$) on day 7 and day 14 post-injection (p.i.). Mean ± SD, statistical significance was calculated using repeated measures ANOVA test. $^{**}P < 0.01$, $^{***}P < 0.001$. (*D*) Serum anti-insulin IgM concentrations of WT mice i.p. injected with PBS (control injection; CI, $n = 5$) and cInsulin ($n = 3$) on day 7 p.i. measured by ELISA at indicated days (coating: native insulin). Mean ± SD, statistical significance was calculated using Mann–Whitney *U* test. $^{*}P < 0.05$. (*E*) Blood glucose levels of WT mice i.p. injected with PBS (CI, $n = 5$) or cInsulin ($n = 5$) on day 0 and day 21 followed by i.v. injections of 100 μg anti-insulin IgM^{high} or 100 μg IgM ctrl on days 22 through 26. Mean ± SD, statistical significance was calculated using repeated measure ANOVA test. $^{*}P < 0.05$, $^{**}P < 0.01$. (*F*) Flow cytometric analysis of mice i.p. injected with PBS (CI, $n = 5$) or cInsulin ($n = 5$/group) together with i.v. injections of 100 μg anti-insulin IgM^{high} or 100 μg IgM control. Panels show pancreatic macrophages (CD11b^{+}) and neutrophils (Ly6G^{+}) pregated on viable cells (fixable viability dye^{-}). Images are representative of three independent experiments. (*G*) Serum pancreatic lipase levels of WT mice i.p. injected with PBS (CI, $n = 5$) and cInsulin ($n = 5$/group) together with i.v. injections of 100 μg anti-insulin IgM^{high} or 100 μg IgM control. Mean ± SD, statistical significance was calculated using Kruskal–Wallis test. $^{*}P < 0.05$, $^{**}P < 0.01$. (*H*) Flow cytometric analysis of bead-based phagocytosis assay performed with high- and low-affinity human anti–Insulin-IgM (IgM^{low} $n = 10$, IgM^{high} $n = 10$) preincubated with dsDNA. Representative zebra plots are on *Left*, and quantitative analysis normalized to IgM^{high} is on *Right*. Mean ± SD, statistical significance was calculated using Mann–Whitney *U* test. $^{***}P < 0.001$.

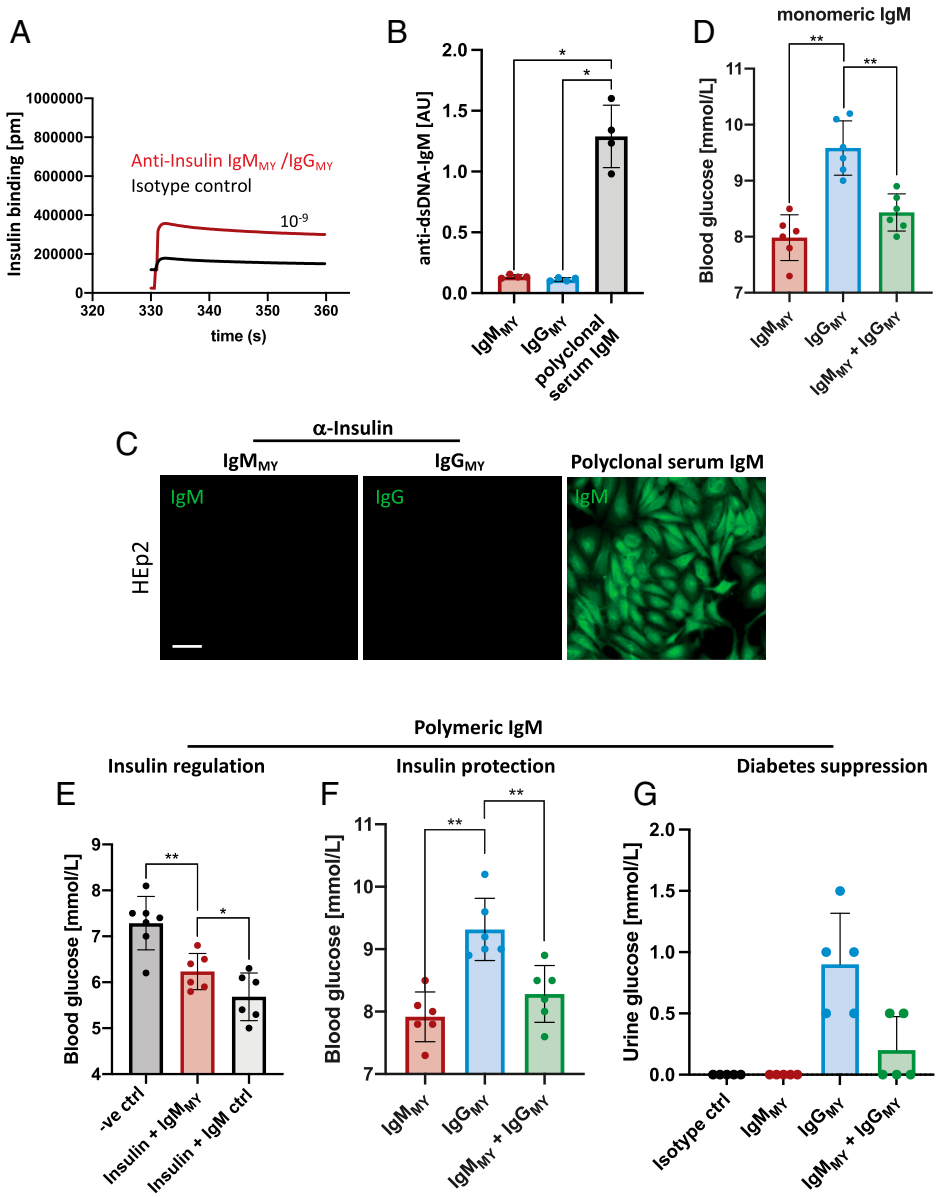

Fig. 4. Monoclonal human insulin-IgM is able to protect insulin in vivo. (*A*) Insulin-binding affinity of monoclonal human anti-insulin Ig determined by BLI. The K_d (dissociation constant) was calculated by using the K_a (association constant): $1/K_a$. Shown data are representative for three independent experiments performed in three dilution steps per sample. (*B*) Anti-dsDNA IgM concentration of insulin-specific IgM pulldowns as measured by ELISA (coating: calf-thymus DNA). IgM$_{MY}$ ($n = 4$), IgG$_{MY}$ ($n = 4$), and polyclonal serum IgM (positive control, $n = 4$). Mean ± SD, statistical significance was calculated using Kruskal–Wallis test. $^*P < 0.05$. (*C*) HEp-2 slides showing anti-nuclear structure-reactive (ANA) monoclonal IgM$_{MY}$ ($n = 6$), IgG$_{MY}$ ($n = 6$), and polyclonal serum IgM (positive control, $n = 6$). (Scale bar: 10 μm.) Green fluorescence indicates HEp-2 cell binding. Images are representative of three independent experiments. (*D*) Blood glucose levels of WT mice i.v. injected with 100 μg monomeric IgM$_{MY}$ ($n = 6$), IgG$_{MY}$ ($n = 6$), and both combined ($n = 6$) 2 h post-injection. Mean ± SD, statistical significance was calculated using Kruskal–Wallis test. $^{**}P < 0.01$. (*E*) Blood glucose levels of WT mice i.v. injected with PBS (−ve ctrl, $n = 7$), 500 ng insulin with 100 μg polymeric IgM$_{MY}$ ($n = 6$) and 500 ng insulin with IgM control ($n = 6$) 2 h post-injection. Mean ± SD, statistical significance was calculated using Kruskal–Wallis test. $^*P < 0.05$, $^{**}P < 0.01$. (*F*) Blood glucose levels of WT mice i.v. injected with 100 μg polymeric IgM$_{MY}$ ($n = 6$), IgG$_{MY}$ ($n = 6$), and both combined ($n = 6$) 2 h post-injection. Mean ± SD, statistical significance was calculated using Kruskal–Wallis test. $^{**}P < 0.01$. (*G*) Urine glucose levels of WT mice immunized with cInsulin and i.v. injected with 100 μg IgM control ($n = 6$), 100 μg polymeric IgM$_{MY}$ ($n = 5$), 100 μg IgG$_{MY}$ ($n = 5$), and both combined ($n = 5$) every 24 h. Measurement shows 8 d post-injection. Mean ± SD, statistical significance was calculated using Kruskal–Wallis test. All comparisons were not significant (n.s.).

antibody function is thought to result in the neutralization of the target antigen. We refer to the generation of a protective antibody as adaptive tolerance because, in contrast to the destructive primary IgM, PR-IgM is generated in the course of secondary immune responses and affinity maturation. We expect canonical B-2 B cells to be the origin of the primary autoreactive neutralizing IgM responses, which are usually short lived. After affinity maturation, long-lived PR-IgM is most likely produced by conventional IgM$^+$/CD27$^+$ memory B cell–derived plasma cells or circulating splenic marginal zone B cells (51, 52). Our data suggest that the ratio of soluble (monovalent) to complex (polyvalent) antigen dictates the outcome of antibody class and that increased monovalent antigen favors the generation of memory IgM over IgG. It remains to be investigated whether these IgM memory B cells in mice and humans are germinal center derived.

In full agreement, our results show that anti-insulin antibody responses are induced by polyvalent insulin complexes generated by chemical cross-linking via carbon–sulfur bonds and independent of any additional adjuvants. SH group–containing drugs are used as immunosuppressive medication [Azathioprine (53)], antilymphoma treatment [Alethine (54)], or acute bronchitis treatment [Erdosteine (55)]. Strikingly, their use was reported to result in the development of anti-insulin autoantibodies (39, 41). Reactive SH groups mediate the generation of protein complexes by the formation of disulfide or carbon–sulfur bonds under oxidizing conditions (56). It is tempting to speculate that peptide hormones such as insulin or other proteins containing free SH groups are disposed to complex formation under oxidative stress when the concentration of oxidants in the body exceeds the capacity of physiologically present antioxidants that balance oxidative stress. Thus, the anti-insulin antibody response induced in this study by oxidative cross-linking of insulin might mimic the physiological conditions which lead to autoantibody production. The oxidative stress-mediated cross-linking of insulin together with the increased amount of misfolded or abnormally cross-linked insulin peptides under conditions of elevated insulin production might lead to recurrent antibody responses against insulin. An inability of the immune system to generate PR-IgM by adaptive tolerance might represent the first step in the development of metabolic disorders associated with blood glucose. According to this scenario, T1D develops when anti-insulin IgG production exceeds or replaces PR-IgM production, resulting in the failure to protect insulin and to prevent pancreas damage. On the other hand, in type 2 diabetes, the production of PR-IgM may decline because of the decreasing generation of new B cells with age (57, 58). In full agreement, the ratio of high-affinity anti-insulin IgM is highly increased in healthy aged humans as compared to young individuals. Thus, a broad B cell repertoire seems to be important for controlling autoimmunity since high-affinity protective IgM has to be produced against virtually every self-structure in order to protect it from self-destructive low-affinity IgM or IgG. This might explain the common relationship between immunodeficiency and autoimmunity (59).

Another important conclusion of our study is that antibodies are not only required for protection from pathogens. Antibodies can also regulate the amount of key physiological factors in the blood such as insulin and are thus important regulators of metabolism and physiology. In addition to the production rate and consumption by target cells, the insulin concentration seems to be regulated by the equilibrium of protective and destructive autoantibodies. In this scenario, protective IgM acts as reservoir that makes insulin quickly accessible while anti-insulin IgG or low-affinity IgM neutralizes the excess of insulin. Our data are supported by experiments showing that high-fat-diet mice (HFD) receiving a B cell–depleting therapy (anti–CD20-IgG) went from hyperglycemic to normoglycemic, suggesting that autoreactive antibodies represent an important part in the development of diabetes and the regulation of metabolism (60). Moreover, the study presented a unique panel of IgG autoantibodies involved in insulin resistance in patients, underlining the importance of glucose metabolism-regulating autoantibodies (60).

This view is further supported by studies reporting severe metabolic disorders in immunodeficiency patients (61). Indeed, CVID patients with drastic hypoglobulinemia showed signs of dysglycemia and defects in fatty acid metabolism (61, 62). In full agreement, our study shows that antibody-deficient mice suffer from dysglycemia and that injecting total IgG or insulin-reactive autoantibodies results in the normalization of blood glucose levels. It remains to be investigated if severe combined immunodeficiency patients, who completely lack B cells and show pan-hypogammaglobulinemia, show dysregulation of blood glucose homeostasis because of the absence of regulatory autoantibodies.

Most likely, other peptide hormones or self-structures are similar to insulin regulated by autoantibodies. Methods for the immortalization of memory B cells can be used for the characterization of protective IgM antibodies (63). Alternatively, converting an autoantigen-specific IgG into IgM-class antibodies might open new venues for the treatment of human autoimmune disorders by protecting the autoantigen. This might create an opportunity to turn ongoing autoimmune diseases into remission. In full agreement, we show that by converting a previously described anti-insulin IgG into IgM reversed its function from an insulin-neutralizing into a protecting agent.

A further conclusion of our findings is that the highly autoreactive primary IgM repertoire represents a high risk for autoreactive damage if high-affinity PR-IgM cannot be generated by secondary immune responses and somatic hypermutation. This suggests that the memory IgM repertoire consists mostly of PR-IgM generated in the course of adaptive tolerance. This also suggests that the defects in somatic hypermutation lead to failure in PR-IgM generation and autoimmune damage induced by the primary IgM. In full agreement, all forms of hyper IgM syndrome (HIGM) are associated with severe autoimmunity (59, 64–66). HIGM patients are particularly prone to developing IgM-mediated autoimmune diseases such as immune thrombocytopenia, hemolytic anemia, and nephritis (65, 67, 68). Notably, autoreactive IgM antibodies that cause autoimmune diseases in HIGM patients are always unmutated and therefore of low affinity to autoantigens (67). These studies report an excessive pathogenic potential of low-affinity autoreactive IgM leading to manifest and severe autoimmunity supporting our concept of neutralizing (low-affinity) and protective (high-affinity) autoreactive IgM.

Together, our findings demonstrate an important role for autoantibodies in physiological homeostasis and suggest that adaptive tolerance is a key mechanism for maintaining physiological integrity.

Materials and Methods

Mice. Female 8- to 15-wk-old C57BL/6 mice (WT) and mb1-deficient mice (69) were intraperitoneally (i.p.) or i.v. injected with samples containing antigens or antibodies in 1× phosphate-buffered saline (PBS). Control injection mice received PBS in a total volume of 100 μL/mouse. We used the following molecules and concentrations for i.v. and i.p. injections: total murine IgG (200 μg/mouse i.v.), commercial human IVIg (200 μg/mouse i.v.), human insulin-specific IgM isolated from serum (100 μg/mouse i.v.), cInsulin (20 μg/mouse i.p.), insulin-bio:streptavidin complexes (20 μg/mouse i.p.), native insulin (0.5 μg/mouse i.p.), monoclonal insulin-specific IgM (100 μg/mouse. i.v.), and monoclonal insulin-specific IgG (100 μg/mouse i.v.). The animal experiments were performed in compliance with the guidelines of German law and were approved by the Animal Care and Committees of Ulm University and the local government under the license number 1484. All mice used in this study were either bred and housed within the animal facility of Ulm University under specific pathogen-free conditions (mb1-deficient mice) or obtained from Charles River at 6 wk of age (WT mice).

Cross-linking of Native Insulin. Native human insulin (Merck) was prediluted in 1% dimethyl sulfoxide (in H_2O) to 1 mg/mL. Chemical carbon–sulfur-cross-linking of thiol groups was achieved by using 1,2-phenylen-bis-maleimide (13118–04-2) at 100 μg/mL for 48 h at room temperature in the dark. Afterward, excess 1,2-phenylen-bis-maleimide was removed by using a 10-kDa cut-off spin column (Abcam, ab93349). Purified insulin complexes (cInsulin) were used for i.p. injections. Quality control was done by using a nonreducing SDS-PAGE and Coomassie staining or blue native (BN)-PAGE.

Macrophage Phagocytosis Assay. The effect of IgM^{high} and IgM^{low} on the antibody-mediated clearance was assessed in mouse phagocytic J774A.1 cell line. Red fluorescent latex beads (2 μm in diameter, Sigma-Aldrich) were coated with purified IgM^{high} and IgM^{low} in a 1:7 ratio and incubated for 45 min at 37 °C. IgM promotes the clearance of small particles and apoptotic microparticles by macrophages (44). The IgM-coated latex beads were

suspended in serum-free culture medium and added to J774A.1macrophages at a 5:1 ratio. After 180-min incubation, the cells were washed in PBS to remove nonengulfed beads. The cells were detached with trypsinization and fixed in 4% paraformaldehyde and subsequently analyzed with a BD LSR II flow cytometer. The macrophage population was identified as described before (70), and the proportion of macrophages containing ingested particles was determined based on the fluorescent signal of the ingested latex beads.

Flow Cytometry. The detailed description is available in ref. 11. Briefly, cell suspensions were Fc receptor blocked with polyclonal rat IgG-UNLB (2,4G2; BD) and stained according to standard protocols. Viable cells were distinguished from dead cells by using Fixable Viability Dye eFluor780 (eBioscience), and stained cells were acquired at a Canto II Flow Cytometer (BD).

ELISA. Antigen-specific ELISAs are described in ref. 28 in detail. Briefly, 96-well plates (Nunc, Maxisorp) were coated with 10 μg/mL native insulin (Sigma-Aldrich, catalog no. [cat.] 91077C) or 2.5 μg/mL calf thymus dsDNA (Thermo Scientific, cat.15633019). Standard coating was done by using anti-IgM, anti-IgG-antibodies (SouthernBiotech). The relative concentrations stated as an arbitrary unit or absolute concentration (μg/mL) were determined via detection by alkaline phosphatase (AP)-labeled anti-IgM/anti-IgG (SouthernBiotech) by using p-nitro-phenylphosphate (Genaxxon) in diethanolamine buffer, respectively.

Enzyme-Linked Immuno-Spot Assay (ELISpot). Total splenocytes were measured in triplicates with cell numbers stated in the figure. ELISpot plates were coated with native Insulin (Sigma-Aldrich, cat. 91077C), anti-IgM (Mabtech), or anti-IgG (Mabtech). Seeded cells were incubated for 12 to 24 h at 37 °C, and antigen-specific IgM or IgG was detected via anti-IgM-bio and SAV-AP or anti–IgG-bio and SAV-AP (Mabtech). The experiments were performed according to the manufacturer's instructions.

HEp-2 Slides and Fluorescence Microscopy. HEp-2 assays with corresponding autoantibodies are described in ref. 28 in detail. Briefly, serum samples indicated in the figures or figure legends were diluted to an equal concentration of IgM (approximately 300 ng/mL anti–Insulin-IgM in both immunized samples) and applied onto the HEp-2 slides (EUROIMMUN, F191108VA). Anti—IgM-APC (allophycocyanin) (eBioscience) and anti–IgG-APC (eBioscience) were used for the visualization of ANA-IgM/-IgG.

Glucose Level Monitoring and Insulin Concentration Determination. The assessment of blood and urine glucose levels is described in ref. 28 in detail. Briefly, we used an Accu Chek (Roche Diagnostics) blood glucose monitor (mmol/L) and took blood from the tail vein. Serum or blood insulin concentrations of human and mouse samples were determined by using commercial ELISA kits by Crystal Chem (mouse: no. 90080, human: no. 90095) according to the manufacturers protocol.

SDS-PAGE and BN-PAGE. The samples were separated on 10 to 20% SDS-polyacrylamide gels, which were incubated with Coomassie (Coomassie brilliant blue R-250, Thermo Fisher) for 45 min and subsequently de-stained. In order to visualize native protein complexes, we used BN-PAGES (SERVA) with BN buffer (1:1 sample to buffer).

Pulldown of Total Serum Immunoglobulins. The serum of injected mice was collected immediately after euthanasia at the indicated days. The antigen bound to antibodies was removed by repeated freeze–thaw cycles of the serum and pH shift during elution (71). Protein G Sepharose beads (Thermo Fisher) were used according to the manufacturer's protocol and obtained antibodies dialyzed overnight in 10 times sample volume of 1× PBS. For isolation of IgM, HiTrap IgM columns (GE Healthcare, Sigma-Aldrich) were used according to the manufacturer's protocol and dialyzed overnight in 10 times sample volume of 1× PBS. The quality of the isolated immunoglobulins was checked via SDS-PAGE and Coomassie staining, and the concentration of antigen-specific immunoglobulins was determined by ELISA.

Isolation of Antigen-Specific Immunoglobulins. Streptavidin bead columns (Thermo Scientific, cat. 21115) were loaded with 10 μg bio-insulin (BioEagle) in order to isolate insulin-specific immunoglobulins. The samples (sera or isolated antibodies) were incubated for 90 min at room temperature to ensure sufficient binding of antibodies to the insulin-loaded beads. The purification of the insulin antibodies was achieved by a pH shift (pH 2.8) using the manufacturer's elution and neutralization solutions. Note, the fractionation into low- and high-affinity fractions was done by eluting with pH 5 (low affinity) and subsequently with pH 2.8 (high affinity). The quality of the isolated immunoglobulins was determined via reduced and nonreduced Coomassie-stained SDS-PAGEs and the quantity determined by ELISA. For further in vivo experiments, the isolated antibodies were dialyzed as described in *Pulldown of Total Serum Immunoglobulins*).

BLI. Interferometric assays (BLItz device, ForteBio) were used to determine the affinity of protein–protein interactions (72) as described in ref. 28.

Wire-Hanging Test. The linear wire-hanging test was used to assess the motor strength and function of mice (73). Individual mice were put onto a 36-cm elevated horizontal wire above a cage; subsequently, the mice tried to stay on the wire by using their paws and muscle strength. The ability in time (seconds) of each mouse to stay on the wire was recorded. A maximum time duration of 240 s was set. Each mouse went through the test three times in a row. The mean value was calculated from the measured data. Blood glucose values were determined before and after the test.

Rotarod Test. To assess motor function and blood glucose levels after physical exercise, the rotarod test was performed (74). Before the start of the experiment, the blood glucose level of the mice was determined. Afterward, they were placed on the running drum of the Rotarod apparatus with a continuous rotation of 32 rpm. At 30 s, the experiment was stopped, and the blood glucose values were measured.

Statistical Analysis. Graphs were created and statistically analyzed by using GraphPad Prism (version 9.1.2) software. The numbers of individual replicates or mice (*n*) are stated within the figure legends. Datasets were preanalyzed by a D'Agostino and Pearson omnibus normality test and/or a Shapiro–Wilk normality test to determine if the values were normally distributed. If one of the datasets was not normally distributed or the sample number *n* was too small to perform the normality tests, nonparametric tests were used to calculate *P* values. In this study, *P* values were calculated by tests stated in the respective figure legends. Student's *t* tests with Welch's correction were used to compare two groups within one experiment. P values > 0.05 were considered to be statistically significant (n.s. = not significant; $*P < 0.05$; $**P < 0.01$; $***P < 0.001$, $****P < 0.0001$).

Data Availability. All study data are included in the article and/or supporting information.

ACKNOWLEDGMENTS. We thank the group of T. Böckers for the free use of the mouse behavior experimental room and M. Reth for critical reading and fruitful discussion. Furthermore, we thank Ina Harder for the serum sampling of immunodeficiency patients. This work was supported by the Deutsche Forschungsgemeinschaft (DFG) through TRR130 (B cells and beyond) project 01, SFB1074 (Experimental Models and Clinical Translation in Leukemia), SFB 1279 (Exploration of the Human Peptidome), and DFG Single Grant JU 463/5-1.

1. H. Modell *et al.*, A physiologist's view of homeostasis. *Adv. Physiol. Educ.* **39**, 259–266 (2015).
2. B. Crimeen-Irwin, K. Scalzo, S. Gloster, P. L. Mottram, M. Plebanski, Failure of immune homeostasis—The consequences of under and over reactivity. *Curr. Drug Targets Immune Endocr. Metabol. Disord.* **5**, 413–422 (2005).
3. N. Hozumi, S. Tonegawa, Evidence for somatic rearrangement of immunoglobulin genes coding for variable and constant regions (K-chain mRNA/restriction enzymes/RNA*DNA hybridization). *Proc. Natl. Acad. Sci. U.S.A.* 73, 3628–3632 (1976).
4. D. B. Roth, V(D)J recombination: Mechanism, errors, and fidelity. *Microbiol. Spectr.*, https://doi.org/10.1128/microbiolspec.MDNA3-0041-2014 (2014).
5. T. Tsubata, M. Reth, The products of pre-B cell-specific genes (λ 5 and VpreB) and the immunoglobulin mu chain form a complex that is transported onto the cell surface. *J. Exp. Med.* **172**, 973–976 (1990).
6. D. Gay, T. Saunders, S. Camper, M. Weigert, Receptor editing: An approach by autoreactive B cells to escape tolerance. *J. Exp. Med.* **177**, 999–1008 (1993).
7. D. Nemazee, K. Buerki, Clonal deletion of autoreactive B lymphocytes in bone marrow chimeras. *Proc. Natl. Acad. Sci. U.S.A.* **86**, 8039–8043 (1989).
8. C. C. Goodnow *et al.*, Altered immunoglobulin expression and functional silencing of self-reactive B lymphocytes in transgenic mice. *Nature* **334**, 676–682 (1988).
9. K. Pieper, B. Grimbacher, H. Eibel, B-cell biology and development. *J. Allergy Clin. Immunol.* **131**, 959–971 (2013).
10. R. Übelhart *et al.*, Responsiveness of B cells is regulated by the hinge region of IgD. *Nat. Immunol.* **16**, 534–543 (2015).
11. C. S. Setz *et al.*, Pten controls B-cell responsiveness and germinal center reaction by regulating the expression of IgD BCR. *EMBO J.* **38**, e100249 (2019).
12. S. B. Hartley *et al.*, Elimination from peripheral lymphoid tissues of self-reactive B lymphocytes recognizing membrane-bound antigens. *Nature* **353**, 765–769 (1991).
13. J. Roes, K. Rajewsky, D. Immunoglobulin, Immunoglobulin D (IgD)-deficient mice reveal an auxiliary receptor function for IgD in antigen-mediated recruitment of B cells. *J. Exp. Med.* **177**, 45–55 (1993).
14. T. Amendt *et al.*, Primary immune responses and affinity maturation are controlled by IgD. *Front. Immunol.* **12**, 709240 (2021).

15. Y. Hao, P. O'Neill, M. S. Naradikian, J. L. Scholz, M. P. Cancro, A B-cell subset uniquely responsive to innate stimuli accumulates in aged mice. *Blood* **118**, 1294–1304 (2011).
16. M. P. Cancro, Age-associated B cells. *Annu. Rev. Immunol.* **38**, 315–340 (2020).
17. A. Kaul *et al.*, Systemic lupus erythematosus. *Nat. Rev. Dis. Primers* **2**, 16039 (2016).
18. C. E. Taplin, J. M. Barker, Autoantibodies in type 1 diabetes. *Autoimmunity* **41**, 11–18 (2008).
19. K. Itoh *et al.*, Clonal expansion is a characteristic feature of the B-cell repetoire of patients with rheumatoid arthritis. *Arthritis Res.* **2**, 50–58 (2000).
20. P. M. Johnson, W. P. Faulk, Rheumatoid factor: Its nature, specificity, and production in rheumatoid arthritis. *Clin. Immunol. Immunopathol.* **6**, 414–430 (1976).
21. J. S. Smolen *et al.*, Rheumatoid arthritis. *Nat. Rev. Dis. Primers* **4**, 18001 (2018).
22. H. Zhang *et al.*, Serum IgG subclasses in autoimmune diseases. *Medicine (Baltimore)* **94**, e387 (2015).
23. C. Franceschi, P. Garagnani, G. Vitale, M. Capri, S. Salvioli, Inflammaging and 'Garbaging'. *Trends Endocrinol. Metab.* **28**, 199–212 (2017).
24. J. Suurmond, B. Diamond, Autoantibodies in systemic autoimmune diseases: Specificity and pathogenicity. *J. Clin. Invest.* **125**, 2194–2202 (2015).
25. M. Boes, Role of natural and immune IgM antibodies in immune responses. *Mol. Immunol.* **37**, 1141–1149 (2000).
26. C. Grönwall, J. Vas, G. J. Silverman, Protective roles of natural IgM antibodies. *Front. Immunol.* **3**, 66 (2012).
27. D. Tsiantoulas, S. Gruber, C. J. Binder, B-1 cell immunoglobulin directed against oxidation-specific epitopes. *Front. Immunol.* **3**, 415 (2013).
28. T. Amendt, H. Jumaa, Memory IgM protects endogenous insulin from autoimmune destruction. *EMBO J.* **40**, e107621 (2021).
29. M. A. Weiss, The structure and function of insulin: Decoding the TR transition. *Vitam. Horm.* **80**, 33–49 (2009).
30. A. Katsarou *et al.*, Type 1 diabetes mellitus. *Nat. Rev. Dis. Primers* **3**, 17016 (2017).
31. R. A. DeFronzo *et al.*, Type 2 diabetes mellitus. *Nat. Rev. Dis. Primers* **1**, 15019 (2015).
32. E. Hobeika *et al.*, Testing gene function early in the B cell lineage in mb1-cre mice. *Proc. Natl. Acad. Sci. U.S.A.* **103**, 13789–13794 (2006).
33. S. Albin, C. Cunningham-Rundles, An update on the use of immunoglobulin for the treatment of immunodeficiency disorders. *Immunotherapy* **6**, 1113–1126 (2014).
34. C. Buchner, C. Bryant, A. Eslami, G. Lakos, Anti-nuclear antibody screening using HEp-2 cells. *J. Vis. Exp.* **88**, e51211 (2014).
35. H. J. Issaq, T. P. Conrads, G. M. Janini, T. D. Veenstra, Methods for fractionation, separation and profiling of proteins and peptides. *Electrophoresis* **23**, 3048–3061 (2002).
36. B. Arora, R. Tandon, P. Attri, R. Bhatia, Chemical crosslinking: Role in protein and peptide science. *Curr. Protein Pept. Sci.* **18**, 946–955 (2017).
37. X. Hu, F. Chen, Exogenous insulin antibody syndrome (EIAS): A clinical syndrome associated with insulin antibodies induced by exogenous insulin in diabetic patients. *Endocr. Connect.* **7**, R47–R55 (2018).
38. Y. Uchigata, Y. Hirata, Y. Iwamoto, Insulin autoimmune syndrome (Hirata disease): Epidemiology in Asia, including Japan. *Diabetol. Int.* **1**, 21–25 (2010).
39. Y. Uchigata, Y. Eguchi, S. Takayama-Hasumi, Y. Omori, Insulin autoimmune syndrome (Hirata disease): Clinical features and epidemiology in Japan. *Diabetes Res. Clin. Pract.* **22**, 89–94 (1994).
40. L. Haataja *et al.*, Disulfide mispairing during proinsulin folding in the endoplasmic reticulum. *Diabetes* **65**, 1050–1060 (2016).
41. M. Karimi *et al.*, Reactivity of disulfide bonds is markedly affected by structure and environment: Implications for protein modification and stability. *Sci. Rep.* **6**, 38572 (2016).
42. T. N. Vinther *et al.*, Additional disulfide bonds in insulin: Prediction, recombinant expression, receptor binding affinity, and stability. *Protein Sci.* **24**, 779–788 (2015).
43. B. van Lierop *et al.*, Insulin in motion: The A6-A11 disulfide bond allosterically modulates structural transitions required for insulin activity. *Sci. Rep.* **7**, 17239 (2017).
44. M. L. Litvack, M. Post, N. Palaniyar, IgM promotes the clearance of small particles and apoptotic microparticles by macrophages. *PLoS One* **6**, e17223 (2011).
45. F. Uher, I. Dobronyi, J. Gergely, Binding of different ligands to IgM-Fc receptors of rat leucocytes. *Immunology* **45**, 387–393 (1982).
46. Y. Zorina, J. Stricker, A. O. Caggiano, D. C. Button, Human IgM antibody rHIgM22 promotes phagocytic clearance of myelin debris by microglia. *Sci. Rep.* **8**, 9392 (2018).
47. C. A. Ogden, R. Kowalewski, Y. Peng, V. Montenegro, K. B. Elkon, IGM is required for efficient complement mediated phagocytosis of apoptotic cells in vivo. *Autoimmunity* **38**, 259–264 (2005).
48. J. R. Weinstein *et al.*, IgM-dependent phagocytosis in microglia is mediated by complement receptor 3, not Fcα/μ receptor. *J. Immunol.* **195**, 5309–5317 (2015).
49. W. Pan, O. Ogunremi, G. Wei, M. Shi, H. Tabel, CR3 (CD11b/CD18) is the major macrophage receptor for IgM antibody-mediated phagocytosis of African trypanosomes: Diverse effect on subsequent synthesis of tumor necrosis factor α and nitric oxide. *Microbes Infect.* **8**, 1209–1218 (2006).
50. H. Ikematsu, Y. Ichiyoshi, E. W. Schettino, M. Nakamura, P. Casali, VH and Vκ segment structure of anti-insulin IgG autoantibodies in patients with insulin-dependent diabetes mellitus. Evidence for somatic selection. *J. Immunol.* **152**, 1430–1441 (1994).
51. S. Weller *et al.*, Human blood IgM "memory" B cells are circulating splenic marginal zone B cells harboring a prediversified immunoglobulin repertoire. *Blood* **104**, 3647–3654 (2004).
52. M. Seifert, R. Küppers, Human memory B cells. *Leukemia* **30**, 2283–2292 (2016).
53. S. E. Baranzini, Autoimmune disorders. *Genomic Pers. Med.* **2**, 822–838 (2013).
54. L. Wang, L. Rong Li, K. H. Young, New agents and regimens for diffuse large B cell lymphoma. *J. Hematol. Oncol.* **13**, 1–23 (2020).
55. M. Cazzola, I. Floriani, C. P. Page, The therapeutic efficacy of erdosteine in the treatment of chronic obstructive bronchitis: A meta-analysis of individual patient data. *Pulm. Pharmacol. Ther.* **23**, 135–144 (2010).
56. J. M. J. M. Ravasco, H. Faustino, A. Trindade, P. M. P. Gois, Bioconjugation with Maleimides: A useful tool for chemical biology. *Chemistry* **25**, 43–59 (2019).
57. D. Frasca, B. B. Blomberg, Aging affects human B cell responses. *J. Clin. Immunol.* **31**, 430–435 (2011).
58. D. Frasca, A. Diaz, M. Romero, A. M. Landin, B. B. Blomberg, Age effects on B cells and humoral immunity in humans. *Ageing Res. Rev.* **10**, 330–335 (2010).
59. G. Bussone, L. Mouthon, Autoimmune manifestations in primary immune deficiencies. *Autoimmun. Rev.* **8**, 332–336 (2009).
60. D. A. Winer *et al.*, B cells promote insulin resistance through modulation of T cells and production of pathogenic IgG antibodies. *Nat. Med.* **17**, 610–617 (2011).
61. A. Fischer, Human primary immunodeficiency diseases: A perspective. *Nat. Immunol.* **5**, 23–30 (2004).
62. A. D. B. Webster, Metabolic defects in immunodeficiency diseases. *Clin. Exp. Immunol.* **49**, 1–10 (1982).
63. E. Traggiai *et al.*, An efficient method to make human monoclonal antibodies from memory B cells: Potent neutralization of SARS coronavirus. *Nat. Med.* **10**, 871–875 (2004).
64. A. Durandy, Hyper-IgM syndromes: A model for studying the regulation of class switch recombination and somatic hypermutation generation. *Biochem. Soc. Trans.* **30**, 815–818 (2002).
65. M. Hervé *et al.*, CD40 ligand and MHC class II expression are essential for human peripheral B cell tolerance. *J. Exp. Med.* **204**, 1583–1593 (2007).
66. G. J. Arason, G. H. Jorgensen, B. R. Ludviksson, Primary immunodeficiency and autoimmunity: Lessons from human diseases. *Scand. J. Immunol.* **71**, 317–328 (2010).
67. M. R. Barbouche *et al.*, Comprehensive review of autoantibodies in patients with hyper-IgM syndrome. *Cell. Mol. Immunol.* **15**, 610–617 (2018).
68. J. A. Winkelstein *et al.*, The X-linked hyper-IgM syndrome: Clinical and immunologic features of 79 patients. *Medicine (Baltimore)* **82**, 373–384 (2003).
69. R. Pelanda *et al.*, Cre recombinase-controlled expression of the mb-1 allele. *Genesis* **32**, 154–157 (2002).
70. H. Yu *et al.*, Breast milk alkylglycerols sustain beige adipocytes through adipose tissue macrophages. *J. Clin. Invest.* **129**, 2485–2499 (2019).
71. R. Reverberi, L. Reverberi, Factors affecting the antigen-antibody reaction. *Blood Transfus.* **5**, 227–240 (2007).
72. S. Kumaraswamy, R. Tobias, "Label-free kinetic analysis of an antibody-antigen interaction using biolayer interferometry" in *Protein-Protein Interactions: Methods and Applications: Second Edition* (Springer, New York, 2015), pp. 165–182.
73. E. Hoffman, S. J. Winder, A modified wire hanging apparatus for small animal muscle function testing. *PLoS Curr.* **8**, 1e2bec4e78697b7b0ff80ea25a1d38be (2016).
74. R. J. Hamm, B. R. Pike, D. M. O'Dell, B. G. Lyeth, L. W. Jenkins, The rotarod test: An evaluation of its effectiveness in assessing motor deficits following traumatic brain injury. *J. Neurotrauma* **11**, 187–196 (1994).